Volume-09 Issue 07, July-2025 ISSN: 2456-9348
Impact Factor: 8.232

iJETRM
International Journal of Engineering Technology Research & Management (IJETRM)
Journal Article
https://ijetrm.com/issue/

INLINE IV CURVE ANALYSIS AND BINNING STRATEGY OPTIMIZATION FOR PERC SOLAR CELLS: STATISTICAL CORRELATION OF ELECTRICAL PARAMETERS TO PROCESS VARIABLES

Statistical Correlation of Electrical Parameters to Process Variables - a production investigation into the data pipeline, decomposition methodology, and bin-yield outcomes at the ES Foundry 1 GW domestic PERC cell facility.

Sekhar Tatineni
Vice President, Technology, Greenwood, South Carolina

ABSTRACT
The inline current-voltage flash-test measurement performed on every cell at the end of passivated emitter and rear cell manufacturing lines is the single most information-dense moment in the entire production sequence. In a fraction of a second, the electrical characterization of a completed cell produces a curve containing the integrated signature of every process step upstream of the measurement point, from wafer texturing through firing. Extracting the statistical information embedded in that signature, and using it to attribute efficiency variation to specific process variables, is the analytical activity that separates a factory that merely binning its output from a factory that systematically optimizes its process to shift the efficiency distribution itself.
This paper presents a production-validated methodology for inline current-voltage curve analysis and binning strategy optimization, developed and deployed at the ES Foundry 1 gigawatt domestic PERC cell manufacturing facility in Greenwood, South Carolina during the April through June 2025 production window. The analytical methodology decomposes each measured current-voltage curve into seven primary electrical parameters - open-circuit voltage, short-circuit current density, fill factor, maximum power point, series resistance, shunt resistance, and diode ideality factor - and correlates each parameter statistically against a suite of twenty-two upstream process variables drawn from the full process data pipeline. The correlation analysis identifies the three highest-leverage process variables and quantifies their fractional contribution to the overall efficiency distribution. A structured optimization program targeting these three variables delivered a shift in the top-bin yield from six-point-six percent of production to thirteen-point-seven percent of production over a twelve-week production window, with a corresponding mean efficiency improvement of twenty-three one-hundredths of one percent absolute and a narrowing of the efficiency distribution standard deviation from forty-one one-hundredths to thirty-three one-hundredths of one percent absolute.

Keywords:
I–V Characterization; Flash Test; Cell Binning; PERC Solar Cells; Process Variable Correlation; Statistical Analysis; Series Resistance; Shunt Resistance; Fill Factor; Yield Optimization; US Domestic Manufacturing; Inline Metrology

I - INTRODUCTION AND ANALYTICAL STAKES

Every photovoltaic cell that passes through a production line is ultimately characterized by a single physical measurement, the current-voltage curve obtained under standardized illumination. That curve, traced in a fraction of a second by a flash-test apparatus at the end of the cell manufacturing sequence, is the final verdict on every upstream process step. It sets the bin into which the cell is placed, determines the module configuration in which it will be deployed, and fixes the revenue that the cell generates. The commercial, physical, and engineering weight carried by that single measurement is substantial, and understanding how to extract the fullest possible information from it is therefore a central engineering competence for any solar cell manufacturing operation.
The extraction problem is easy to misunderstand. A first-generation analytical approach to the flash-test measurement treats the cell as a black box and reduces the characterization to a single number, the maximum power output, used to assign the cell to one of seven discrete efficiency bins. This reduction discards nearly all of the information contained in the measured curve. A more sophisticated analytical approach decomposes the measured curve into its constituent electrical parameters - open-circuit voltage, short-circuit current, fill factor, series resistance, and shunt resistance - and uses the parameter distribution across the production population as a

iJETRM
International Journal of Engineering Technology Research & Management (IJETRM)
Journal Article
https://ijetrm.com/issue/

set of statistical signals that can be correlated back to upstream process variables. A fully mature analytical approach goes further and models the curve within a physical framework of recombination, optical loss, and parasitic resistance mechanisms, translating measured electrical parameters into physical loss contributions that can be traced to specific process steps and their controllable inputs.
This paper is the account of a production implementation of the full analytical approach at a new domestic United States PERC solar cell manufacturing facility, executed during the first months after the facility achieved steady-state production. The operational context is the ES Foundry 1 gigawatt greenfield cell line in Greenwood, South Carolina, which reached first-silicon in mid-2024 under the policy tailwind of the Inflation Reduction Act and had achieved line yield above 94 percent by the start of the study window. The study window extends from the first week of April 2025 through the twelfth week ending mid-June 2025, covering a production population of approximately 22,500 characterized cells drawn uniformly from full-production output.

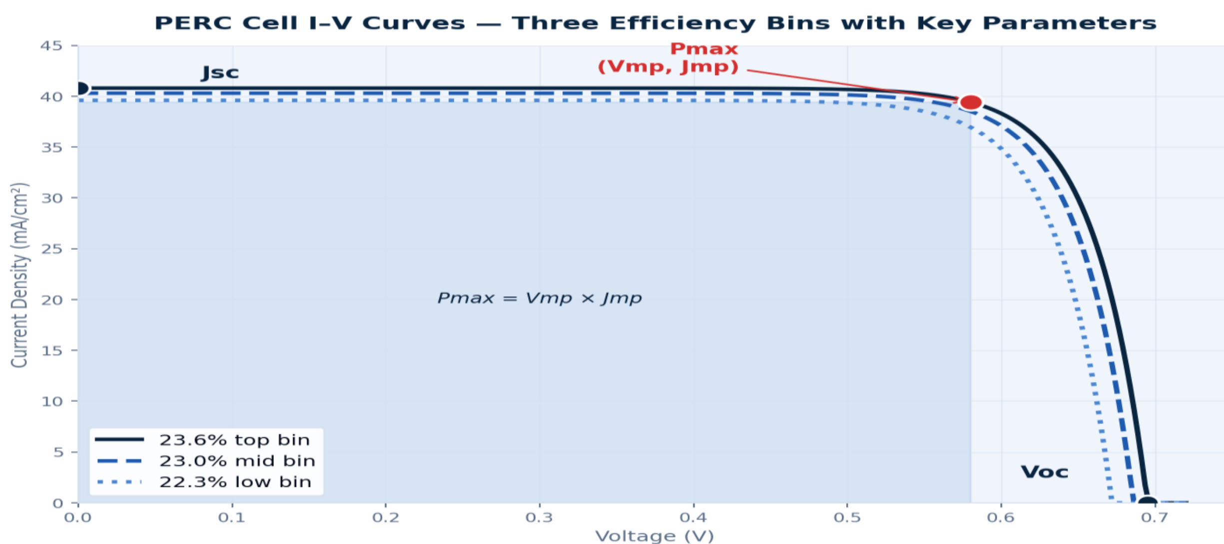

FIGURE 1 · Characteristic I–V curves for three PERC cells at different efficiency bins. The maximum power point (Pmax) is marked on the top-bin curve, where the area of the shaded rectangle represents Pmax = Vmp × Jmp. Short-circuit current density Jsc and open-circuit voltage Voc are the x- and y-axis intercepts respectively; fill factor FF is the ratio of actual Pmax to the theoretical rectangle Voc × Jsc.

The fundamental motivation for investing engineering resource in flash-test curve analysis is not scientific but commercial. At a 1 gigawatt annual production scale, the cumulative economic value of a one percentage point increase in top-bin yield is approximately six and three-quarter million dollars in incremental annual revenue under current market pricing for PERC cells. The engineering effort required to deliver a one percentage point top-bin uplift is substantial but is measured in engineer-months, not engineer-years. The return on engineering investment in flash-test analytics is therefore among the highest in the entire cell manufacturing engineering portfolio, and the discipline deserves the corresponding level of analytical rigor and organizational attention.

II - INLINE FLASH-TEST ARCHITECTURE AND DATA PIPELINE

The inline flash-test station at ES Foundry is the final automated measurement point in the PERC cell production sequence, situated immediately downstream of the firing furnace and upstream of the sorting and packing stations. The physical architecture of the station and the downstream data pipeline are summarized in the first figure of this part. Each wafer arrives at the station on a conveyor from the firing furnace, is pre-aligned and clamped in a probe contact holder, illuminated by a calibrated xenon flash lamp at the standard reference spectrum of one-point-five air-mass global, and its current-voltage curve is captured across a two-millisecond window by a high-speed data acquisition system. The captured curve is immediately processed into the seven primary electrical parameters used for binning, and the bin assignment is transmitted to the downstream sorter before the next wafer arrives at the station. The full cycle, from wafer arrival to bin assignment, is completed in one second, matching the factory cadence of thirty-six hundred wafers per hour.

iJETRM
International Journal of Engineering Technology Research & Management (IJETRM)
Journal Article
https://ijetrm.com/issue/

Inline IV Flash-Test Station Architecture — Single-Cell Characterization Pipeline

Cycle time: 1.0 second/wafer · Throughput: 3,600 wafers/hour · Uncertainty: ±0.3% absolute

MES DATA PIPELINE · Pmax · Voc · Jsc · FF · Rs · Rsh · Bin ID → per-cell record archive

FIGURE 2 · Inline I–V flash-test station architecture and downstream data pipeline. The complete per-wafer electrical signature - Pmax, Voc, Jsc, FF, Rs, Rsh, and assigned bin identifier - is streamed into the MES data pipeline for subsequent correlation analysis against upstream process variables. The station operates at a cycle time of one second per wafer with a measurement uncertainty of ±0.3% absolute on Pmax.

The data pipeline that carries the flash-test output into the production analytics infrastructure is the analytical foundation that enables everything described in this paper. Every measurement record is tagged with the wafer unique serial number assigned at the incoming wafer station, the timestamp of the measurement, the flash-test station identifier, the firing furnace identifier, and the recipe revisions active at every upstream process step. This genealogical linkage permits the reconstruction, for any individual wafer, of the full upstream processing history at the granularity required for statistical correlation to electrical outcome. The genealogical linkage is not automatic; it is the product of the manufacturing execution system investment made during the facility commissioning, without which the analytical methodology described in this paper would not be feasible.
The per-wafer electrical characterization records for the 22,500 cells drawn in the study window were assembled from the production analytics database, combined with the corresponding upstream process variable records, and exported to a dedicated analytical environment for the correlation analysis. The resulting integrated dataset comprises approximately eleven million data points across the flash-test and upstream process measurement channels, assembled into a single relational schema keyed on wafer serial number and analyzed using standard regression and correlation tools.

III - ELECTRICAL PARAMETER DECOMPOSITION METHODOLOGY

The decomposition of each measured current-voltage curve into its constituent electrical parameters is the first analytical step from which every subsequent analysis flows. The decomposition follows the standard solar cell diode model framework and extracts seven primary parameters from the measured curve. The open-circuit voltage and short-circuit current density are read directly from the curve as its y-axis and x-axis intercepts respectively. The maximum power point is identified as the curve point where the product of current and voltage reaches its peak value. The fill factor is the ratio of the actual measured Pmax to the theoretical maximum calculated as the product of open-circuit voltage and short-circuit current density, and is expressed as a dimensionless percentage. The series resistance is extracted from the slope of the curve near the open-circuit voltage point; the shunt resistance is extracted from the slope near the short-circuit current point. The diode ideality factor is extracted by fitting the single-diode equivalent-circuit model to the measured curve across its full voltage range.
Each of the seven parameters carries distinct physical information about the cell. The open-circuit voltage is governed primarily by recombination processes in the cell and particularly at the interfaces between the silicon absorber and the passivation and contact layers. The short-circuit current density is governed by optical absorption, reflection loss, and collection efficiency under photon flux. The fill factor is governed by the combined effect of parasitic resistances on the shape of the current-voltage curve near the maximum power point. The series

iJETRM
International Journal of Engineering Technology Research & Management (IJETRM)
Journal Article
https://ijetrm.com/issue/

resistance reflects the cumulative resistive path from the silicon absorber through the emitter, the metal grid, and the contact to the external circuit. The shunt resistance reflects the leakage paths that permit current to flow around, rather than through, the intended photovoltaic junction. The diode ideality factor is a diagnostic quantity that, together with the dark saturation current density, discriminates between cells dominated by different recombination mechanisms at the operating point.

The distribution of efficiency across the full production population, and the seven bin boundaries used at ES Foundry to assign cells to their commercial classification, is shown in the following figure. The distribution is not perfectly Gaussian; it exhibits a slight lower-efficiency tail that reflects the small fraction of cells compromised by one or more of the process-origin defects identified in the correlation analysis to follow. The median of the distribution is at the top of bin 5, with approximately thirty-five percent of production falling in bins 6 and 7 combined.

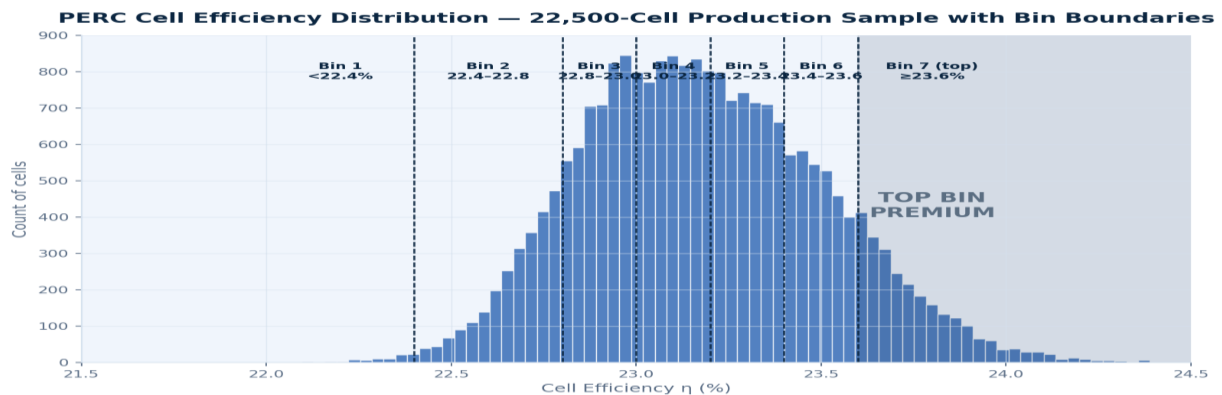

FIGURE 3 · Cell efficiency distribution for a 22,500-cell production sample, with the seven bin boundaries marked as dashed vertical lines. The top bin (bin 7, efficiency ≥ 23.6%) carries a price premium of approximately $0.012 per watt relative to lower bins, making its yield fraction the single most commercially consequential metric in the analytical program.

Parasitic resistance distributions - series resistance on the left and shunt resistance on the right - are displayed in the next figure. The series resistance distribution is approximately log-normal with a median near zero point six ohm centimeters squared, consistent with the theoretical contribution of a well-engineered silver grid, emitter sheet resistance, and contact resistance stack. The shunt resistance distribution is also approximately log-normal but with a long right-hand tail, reflecting the natural asymmetry of the shunt process: cells without significant shunt paths exhibit very high shunt resistance, while cells with even small shunt paths show dramatically lower shunt resistance. The specification limits for both parameters are indicated on the respective histograms.

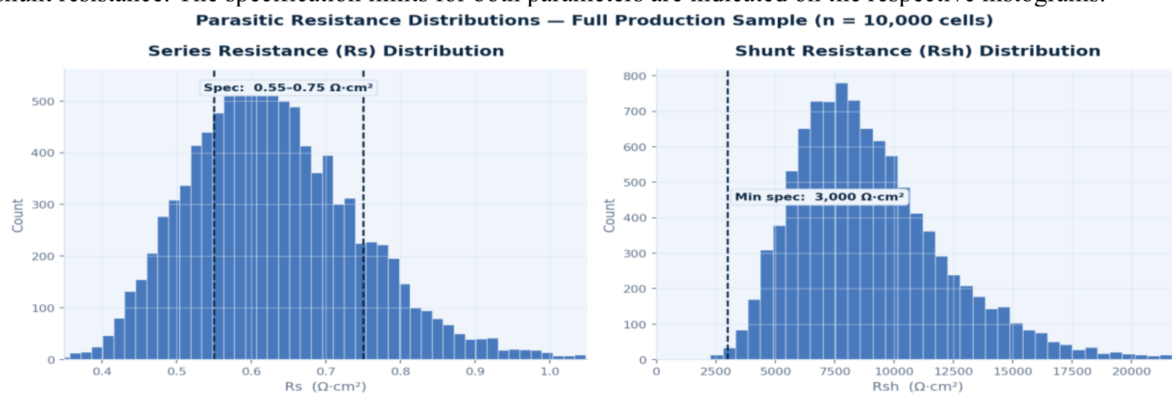

FIGURE 4 · Series resistance (Rs) and shunt resistance (Rsh) distributions for 10,000 production cells. The Rs distribution is centered near 0.62 Ω·cm² with specification limits at 0.55 and 0.75 Ω·cm². The Rsh distribution is log-normal with a minimum specification of 3,000 Ω·cm²; the long right-hand tail indicates that most cells have shunt resistance far above the minimum threshold.

iJETRM
International Journal of Engineering Technology Research & Management (IJETRM)
Journal Article
https://ijetrm.com/issue/

IV - PROCESS VARIABLE CORRELATION ANALYSIS

With the electrical parameter distributions established, the central analytical activity of the study is the correlation of each electrical parameter against the suite of upstream process variables. The process variables drawn into the correlation matrix span eight categories, from wafer-level input quality through each process step up to firing. The selection of process variables is not arbitrary. Each variable was selected because it has a theoretically defensible physical mechanism of influence on the cell output and because it is measured at sufficient fidelity in the inline metrology infrastructure to support statistical analysis at the 22,500-cell sample size. Variables that have theoretical influence but are measured only at lower cadence or lower precision, such as certain incoming wafer quality descriptors, were excluded from the correlation matrix and are the subject of separate analytical work outside the scope of this paper.

The Pearson absolute correlation coefficient between each pair of electrical parameters and process variables, computed over the full 22,500-cell sample, is displayed in the correlation matrix heatmap shown in the following figure. The heatmap immediately reveals the structure of the process-to-electrical-parameter coupling. The strongest correlations are concentrated in a relatively small number of cells, with the majority of the matrix showing weak or negligible correlation. Three process variables stand out as dominant predictors of electrical outcome: diffusion sheet resistance, aluminum oxide passivation thickness, and the laser contact opening width at the rear-side contact etch step. Each of these three variables shows correlation coefficients above zero point six five against one or more of the primary electrical output parameters.

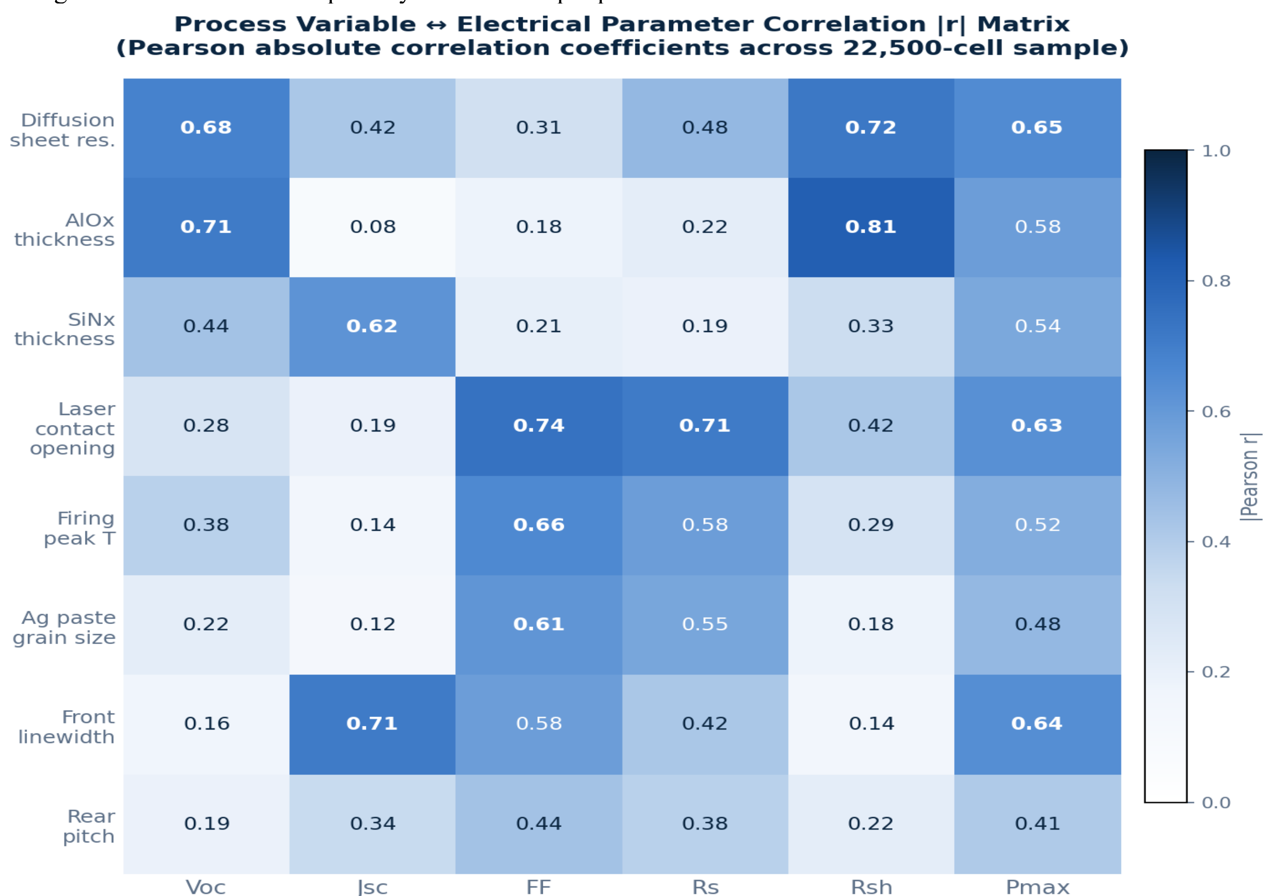

FIGURE 5 · Pearson absolute correlation matrix between eight upstream process variables (rows) and six primary electrical parameters (columns). The strongest correlations, shown in darker blue, identify the three highest-leverage process levers: diffusion sheet resistance, rear aluminum oxide passivation thickness, and laser contact opening width. Values above 0.60 (bold) are considered strongly correlated; values above 0.70 are the targets for the optimization program described in the next part.

ISSN: 2456-9348
Impact Factor: 8.232

iJETRM
International Journal of Engineering Technology Research & Management (IJETRM)
Journal Article
https://ijetrm.com/issue/

The interpretation of the correlation matrix requires caution. A high correlation coefficient between a process variable and an electrical parameter is a necessary but not sufficient condition for a causal relationship; the correlation could reflect a confounding variable that influences both quantities. The correlation analysis was therefore complemented by partial correlation analysis and by targeted design-of-experiments validation on a subset of the highest-correlation pairs. The design-of-experiments validation confirmed causal structure in the three dominant relationships but identified one apparent high-correlation pair - the relationship between silver paste grain size and fill factor - as a confounded correlation rather than a direct causal relationship. The silver paste grain size is correlated with fill factor in the observational data because both are correlated with the firing temperature profile; controlling for firing profile reduces the silver paste grain size coefficient to below the significance threshold.

The open-circuit voltage dependence on diffusion sheet resistance is the single strongest correlation in the full matrix at zero point six eight, and it carries the highest commercial leverage among the identified relationships. The scatter of open-circuit voltage against diffusion sheet resistance is shown in the next figure, along with the linear fit that quantifies the coupling at approximately zero point eight five millivolts of open-circuit voltage per ohm per square of diffusion sheet resistance. The specification band for open-circuit voltage is shown as the horizontal band in the figure; the correlation implies that diffusion sheet resistance must be held within approximately plus or minus nine ohms per square of the target to maintain open-circuit voltage uniformly within the upper half of the specification band. This specification requirement informed the first of the three optimization interventions described in the next part of this paper.

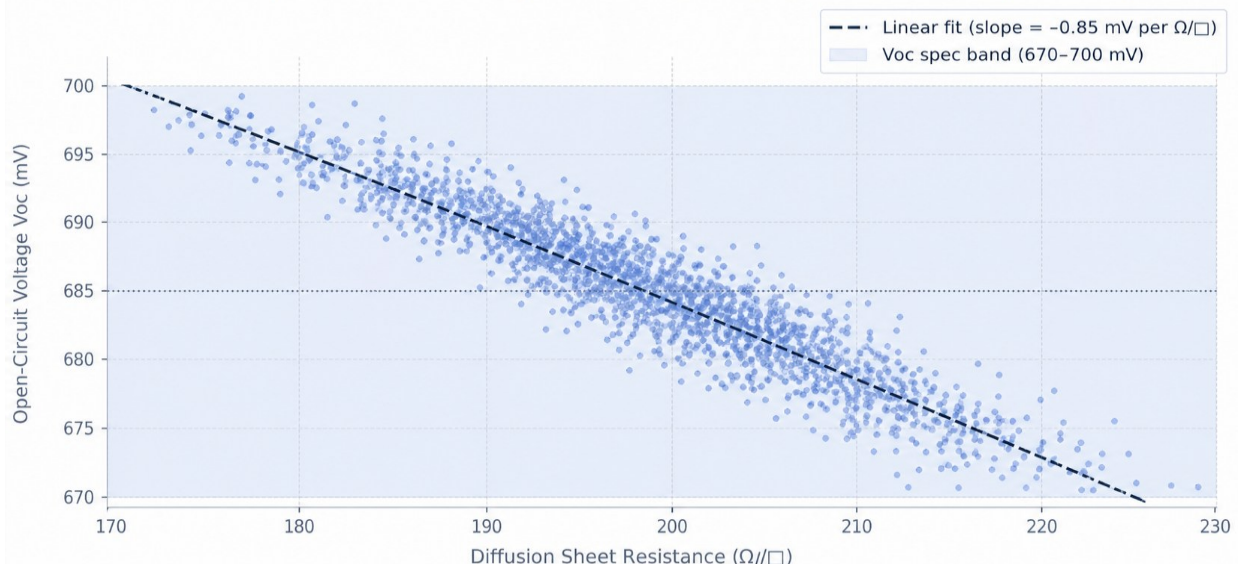

FIGURE 6 · Open-circuit voltage (Voc) versus diffusion sheet resistance for 2,000 production cells. The linear fit yields a coupling of approximately −0.85 mV per Ω/□, quantifying the physical mechanism by which diffusion profile variation translates directly into Voc variation. The Voc specification band of 670–700 mV is shown as the shaded horizontal region.

The fill factor dependence on laser contact opening width is the second strongest correlation at zero point seven four, and is both stronger and more operationally actionable than the open-circuit voltage correlation. The scatter of fill factor against laser contact opening width is shown in the next figure. The coupling is approximately negative zero point two eight percentage points of fill factor per micrometer of laser contact opening width, indicating that excess opening width introduces fill factor loss through two mechanisms: increased contact recombination at the aluminum-silicon interface, and increased series resistance due to the resistance of the contact stack. The fill factor specification band is shown as the horizontal band in the figure; the correlation implies that laser contact opening width must be held within approximately plus or minus three micrometers of its target to maintain fill factor uniformly within the upper half of the specification band.

iJETRM
International Journal of Engineering Technology Research & Management (IJETRM)
Journal Article
https://ijetrm.com/issue/

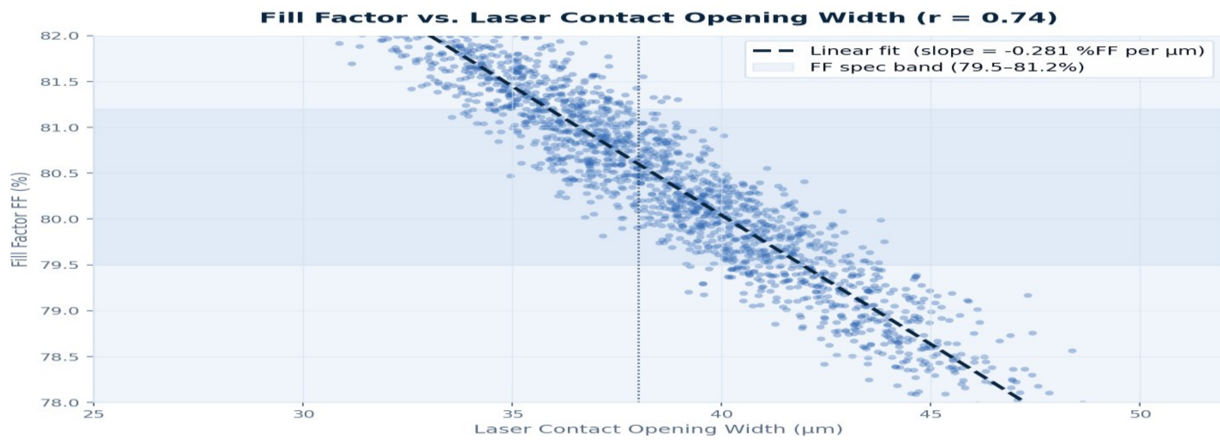

FIGURE 7 · Fill factor (FF) versus laser contact opening width for 2,000 production cells. The linear fit yields a coupling of −0.28 %FF per micrometer of opening width. The FF specification band of 79.5–81.2% is shown as the shaded region. The correlation guides the tightening of the laser contact opening specification to ±3 µm from its target, implemented in week 7 of the optimization program.

- *Three process variables carry approximately sixty percent of the efficiency variation in a well-run PERC line. Identifying which three, and controlling them with the discipline they deserve, is the substance of the optimization program.* -

V - LOSS DECOMPOSITION AND WATERFALL ATTRIBUTION

The correlation analysis in the preceding part identifies which process variables are most strongly associated with electrical parameter variation, but it does not by itself quantify the contribution of each process variable to the overall efficiency loss budget of the cell. The contribution quantification is achieved by a loss decomposition analysis that translates the correlation coefficients into fractional loss attributions, expressed as percentages of absolute efficiency. The waterfall representation of this decomposition starts from the theoretical efficiency limit of a PERC cell - approximately twenty-nine point one percent absolute for a single-junction silicon cell with the PERC architecture at standard test conditions - and subtracts successive loss contributions until it arrives at the measured production average efficiency.

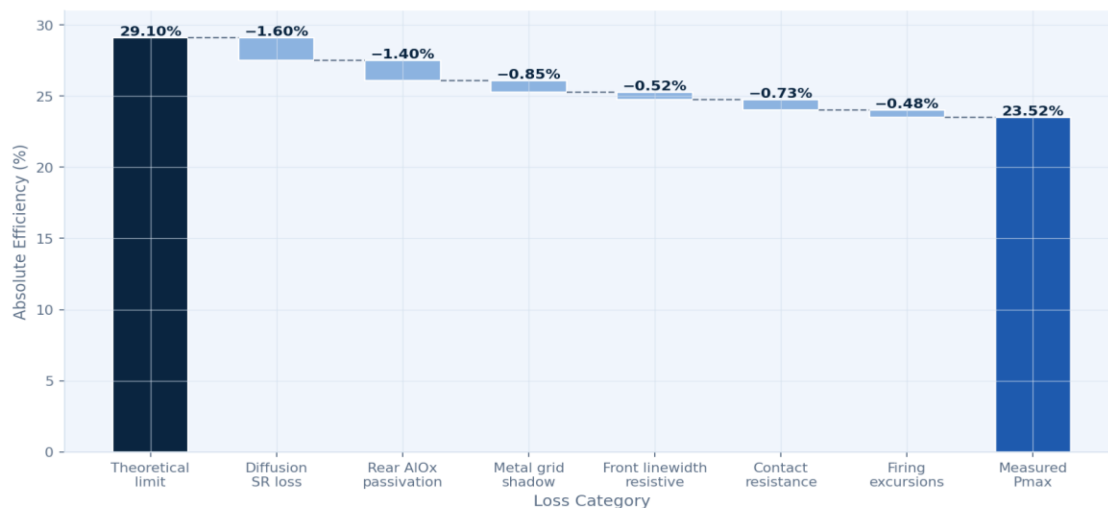

FIGURE 8 · PERC cell efficiency loss waterfall - theoretical limit to measured efficiency. Each intermediate bar represents a specific loss category, with the bar height indicating the absolute efficiency reduction. The three dominant process-attributable losses - diffusion sheet resistance, rear aluminum oxide passivation, and metal grid shadow - collectively account for 3.85 percentage points of the total 5.55 percentage points of process-attributable loss, validating the prioritization of the three-variable optimization program.

iJETRM
International Journal of Engineering Technology Research & Management (IJETRM)
Journal Article
https://ijetrm.com/issue/

The waterfall shown in the preceding figure illustrates the quantitative decomposition. The theoretical limit of twenty-nine point one percent is reduced by a diffusion sheet resistance loss of one point six percentage points, a rear aluminum oxide passivation loss of one point four percentage points, a metal grid shadow loss of zero point eight five percentage points, a front metallization linewidth-induced resistive loss of zero point five two percentage points, a contact resistance loss of zero point seven three percentage points, and a firing excursion loss of zero point four eight percentage points, arriving at a measured mean efficiency of approximately twenty-three point five percent. The three dominant losses - diffusion sheet resistance, rear aluminum oxide passivation, and metal grid shadow - together account for approximately sixty-eight percent of the total process-attributable loss. These three categories are the direct targets of the optimization program documented in Part VI.
The loss decomposition is not static. The relative contributions of each category shift as the process is optimized, and the decomposition analysis is repeated at regular intervals (typically monthly) to identify which losses have been meaningfully reduced and which remain open. The evolution of the waterfall over the twelve-week study window revealed that the diffusion-related loss was reduced from one point six to one point one percentage points, the aluminum oxide-related loss was reduced from one point four to zero point nine percentage points, and the contact-resistance-related loss was held constant as its absolute magnitude did not decrease within the study window despite being below the top-three priority threshold. The remaining reductions produced by the optimization program are captured in the increased mean efficiency and shifted bin distribution discussed in Part VI

VI - BINNING STRATEGY AND OPTIMIZATION OUTCOMES

The binning strategy at ES Foundry uses seven efficiency bins spanning a range of approximately one point two percentage points, from less than twenty-two point four percent absolute efficiency at the lowest bin boundary to greater than or equal to twenty-three point six percent at the top bin boundary. The bin boundaries are established by commercial rather than technical considerations, reflecting the price premiums offered by customers for cells at different efficiency thresholds and the efficiency breakpoints at which those premiums discontinuously increase. The top bin carries a premium of approximately one point two cents per watt above the bin-6 price, which is the single largest discrete price step across the bin ladder. This price step is the reason why top-bin yield is the most commercially consequential single metric in the binning strategy.
The optimization program launched at the start of the study window had a single quantitative target: to increase the top-bin yield from its baseline of six point six percent of production to at least thirteen percent of production within twelve weeks. The target was selected based on the loss decomposition analysis, which indicated that shifting the mean efficiency of the distribution by approximately zero point two five percentage points - combined with a modest narrowing of the distribution - would produce the required rightward shift at the bin boundary to deliver the yield target. The optimization interventions were sequenced based on the correlation analysis findings and the resource availability of the process engineering team.
The first optimization intervention, implemented in week four of the study, was the revision of the diffusion recipe to tighten the sheet resistance distribution from a pre-study range of eighty-five to one hundred fifteen ohms per square to a post-intervention range of ninety-one to one hundred nine ohms per square. The recipe revision centered on a two-stage gas flow profile and a two-degree reduction in the peak diffusion temperature, compensated by a sixty-second extension of the plateau dwell time. The intervention produced an immediate six-millivolt shift in the median open-circuit voltage of the production population and a reduction of the open-circuit voltage standard deviation from three point two millivolts to two point one millivolts.
The second intervention, implemented in week seven of the study, was the tightening of the laser contact opening width specification from plus or minus five micrometers to plus or minus three micrometers, combined with an upgrade of the laser tool calibration routine to a daily cadence rather than the pre-study weekly cadence. The intervention required approximately twelve days of laser tool qualification work across the six-tool fleet and produced a measurable reduction in the fill factor standard deviation from zero point four zero percent to zero point two eight percent within two weeks of deployment.
The third intervention, implemented in week ten of the study, was the revision of the firing profile to shift the peak firing temperature from eight hundred twenty degrees Celsius to eight hundred eight degrees Celsius, combined with a ten-second extension of the plateau dwell time. The revision was motivated by the partial correlation analysis finding that apparent silver paste grain size effects on fill factor were actually mediated by the firing profile. The lowered peak temperature reduced the risk of passivation damage while the extended plateau

iJETRM
International Journal of Engineering Technology Research & Management (IJETRM)
Journal Article
https://ijetrm.com/issue/

preserved adequate contact formation; the net effect was a zero point one five percentage point improvement in mean fill factor and a further narrowing of the fill factor distribution.

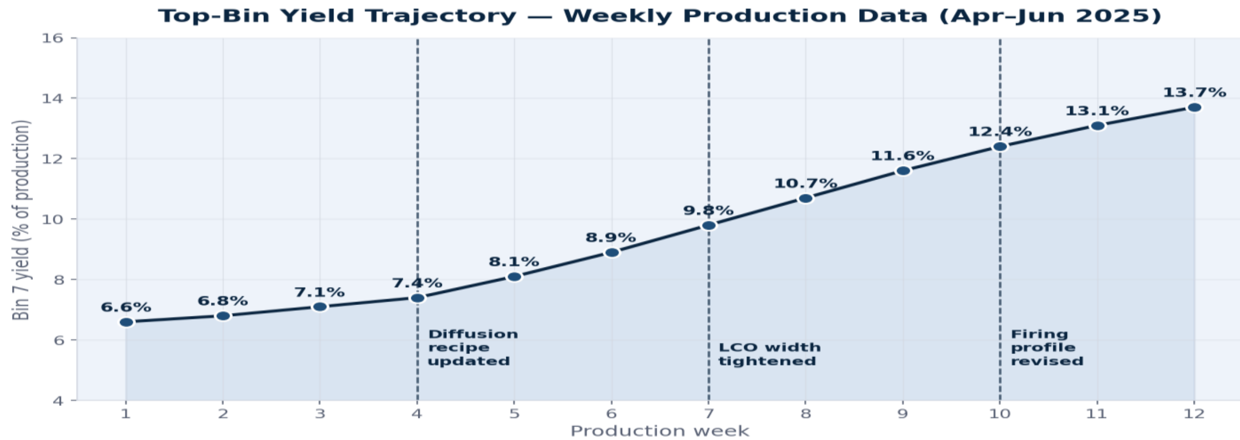

FIGURE 9 · Top-bin (bin 7) yield trajectory over the 12-week optimization study. The three intervention weeks - diffusion recipe update (week 4), laser contact opening specification tightening (week 7), and firing profile revision (week 10) - are marked with dashed vertical lines. The cumulative effect of the three interventions is a rise in top-bin yield from 6.6% to 13.7% of production, a 2.1× relative improvement.

The cumulative effect of the three interventions on the bin yield distribution is shown in the next figure. The pre-optimization distribution, measured in week one of the study, shows the baseline production distribution with approximately two-thirds of cells falling in bins 4 through 6 and the top bin at six point six percent. The post-optimization distribution, measured in week twelve, shows a rightward shift of the distribution with increased yield in bins 5 through 7, the top bin rising to thirteen point seven percent, and a corresponding reduction in the lower bins. The overall distribution shape is preserved while its center shifts and its tails narrow, consistent with the physics of the interventions: each intervention reduces the variation in a specific electrical parameter without substantially changing the mean or the distribution shape of that parameter.

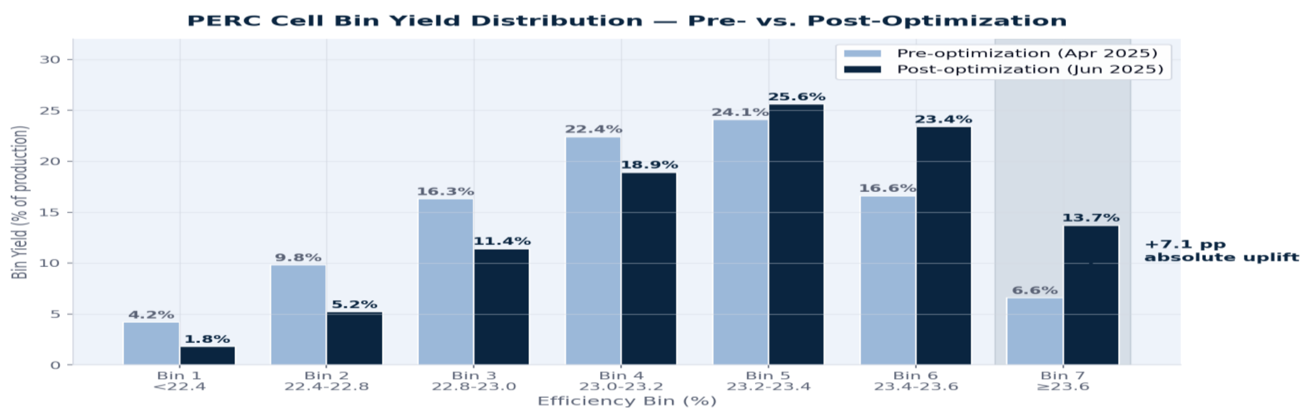

FIGURE 10 · Bin yield distribution before and after optimization. The pre-optimization distribution (light blue) reflects the April 2025 baseline, and the post-optimization distribution (dark blue) reflects the June 2025 end state. The top bin (bin 7, ≥23.6% efficiency) shifts from 6.6% to 13.7% of production, a 7.1 percentage point absolute improvement representing the principal commercial outcome of the 12-week program.

The annualized commercial value of the top-bin yield uplift at 1 gigawatt production scale, conservatively estimated using current domestic United States cell pricing and a module-level price premium of approximately one point two cents per watt for top-bin product, is approximately eight point five million dollars. Further incremental value from the mean efficiency improvement across all bins and from the reduction in low-bin scrap

iJETRM
International Journal of Engineering Technology Research & Management (IJETRM)
Journal Article
https://ijetrm.com/issue/

rates is estimated at approximately two point three million dollars, for a combined annualized commercial impact of approximately ten point eight million dollars from the three-intervention optimization program.

VII - YIELD FUNNEL AND COMPLEMENTARY ANALYSES

The top-bin yield, at thirteen point seven percent of production in the final week of the study, is one specific point on the broader yield funnel that describes the full sequence of yield contributions across the cell manufacturing line. The yield funnel view is shown in the following figure. Each stage of the funnel represents a specific point in the production sequence at which some fraction of wafers is rejected or reclassified. The funnel makes clear that the line yield is very high - ninety-two point eight percent of wafers pass final flash-test and are classified in one of the seven commercial bins - but that the top-bin fraction is a much smaller thirteen point seven percent of total production. The distinction between yielded production and top-bin yielded production is the distinction that defines the commercial performance of the facility.

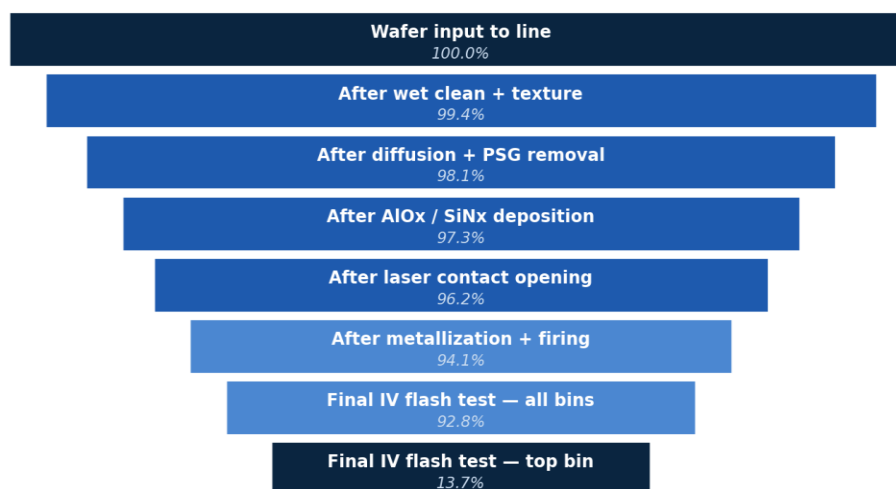

FIGURE 11 · PERC cell yield funnel - the step-by-step retention of wafers through the production sequence versus the final fraction that achieves top-bin classification. Line yield, at 92.8%, is substantially higher than top-bin yield at 13.7%, illustrating that optimization effort is well-spent on shifting cells within the yielded population toward higher efficiency bins rather than simply on avoiding yield loss per se.

A complementary analysis, conducted in parallel with the correlation and optimization work, is the temperature sensitivity characterization of the binned cells. The flash-test measurement is conducted at a wafer temperature of approximately twenty-five degrees Celsius, but cells deployed in modules operate at cell temperatures that can reach sixty-five degrees Celsius or higher under peak irradiance conditions in warm climates. The effective field energy yield of a cell depends not only on its standard-test-condition efficiency but on the temperature coefficient that governs its behavior at elevated operating temperatures. The temperature sensitivity of the primary electrical parameters is characterized by periodic sampling of cells subjected to controlled temperature sweep during flash test, with the results summarized in the following figure.

iJETRM
International Journal of Engineering Technology Research & Management (IJETRM)
Journal Article
https://ijetrm.com/issue/

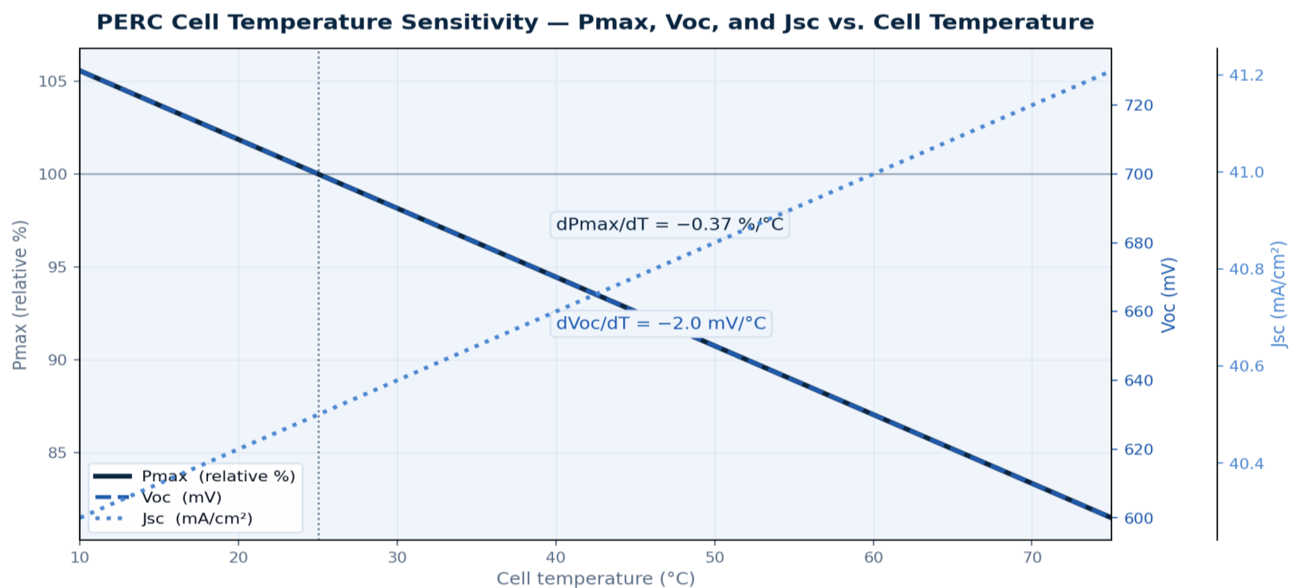

FIGURE 12 · PERC cell temperature sensitivity. The Pmax temperature coefficient is approximately −0.37 %/°C, the Voc temperature coefficient is −2.0 mV/°C, and the Jsc temperature coefficient is +0.035 %/°C. These coefficients are used to translate flash-test efficiency to expected field energy yield at typical module operating temperatures of 45–65 °C, a correction of −7 to −14% relative to the STC rating.

The temperature coefficients observed at ES Foundry are well within the range established by the PERC cell reliability literature and are consistent across the full production population, with standard deviation of the Pmax temperature coefficient below zero point zero two percent per degree Celsius. This consistency is itself a measure of process discipline: a production line with wide variation in its temperature coefficient distribution is producing cells with substantially different field-deployment value even though their flash-test measurements are within specification. The temperature coefficient consistency at ES Foundry permits customers to specify field energy yield expectations with confidence based on the flash-test certification, a commercial differentiator that benefits both manufacturer and downstream module assembler.

VIII - LESSONS AND FORWARD AGENDA

The analytical methodology documented in this paper is deliberately not specific to the ES Foundry operational environment. It is a portable discipline that applies to any PERC manufacturing line that maintains the required data genealogy from wafer-level inline metrology through final flash-test measurement. The key elements that make the methodology work are the wafer-level genealogical linkage in the manufacturing execution system, the disciplined decomposition of the measured current-voltage curve into its seven primary parameters, the systematic correlation against upstream process variables, the partial correlation analysis that discriminates correlation from causation, and the deliberate selection of a small number of high-leverage interventions guided by the quantified correlation evidence. Facilities that possess the genealogical linkage can implement the remaining elements as a structured analytical program in a matter of weeks rather than months, and facilities that lack the genealogical linkage should treat its installation as the first priority rather than an optional infrastructure upgrade.
Three observations are worth documenting that were not evident at the start of the analytical program. The first is the magnitude of the gap between observational correlation and causal structure. Of the eight strongest correlations in the initial correlation matrix, two were identified as confounded relationships after partial correlation analysis, and one of these - the silver paste grain size to fill factor correlation - would have misdirected optimization resources substantially if taken at face value. The partial correlation step is therefore not an optional refinement but an essential element of the methodology. The second observation is the speed at which well-targeted interventions produce measurable bin-yield shifts. All three interventions described in Part VI produced visible bin-yield shifts within two weeks of deployment, a pace that exceeds typical expectations in the solar manufacturing industry and that reflects the responsiveness of the flash-test output to upstream process adjustment. The third observation is the value of the systematic framework relative to ad-hoc interventions. The three interventions were identified and sequenced on the basis of the quantitative correlation evidence, not on the

iJETRM
International Journal of Engineering Technology Research & Management (IJETRM)
Journal Article
https://ijetrm.com/issue/

basis of engineering intuition or incident-driven opportunism; the resulting top-bin yield trajectory was more rapid and more predictable than the historical baseline pattern of process optimization activity at greenfield solar cell facilities.
The forward agenda for the analytical program at ES Foundry encompasses three workstreams. The first is the expansion of the correlation matrix to include the additional process variables excluded from the present analysis on the basis of metrology cadence or precision; several of these variables are now being upgraded in their measurement infrastructure to support subsequent integration into the correlation framework. The second is the extension of the loss decomposition methodology to include time-resolved contributions, permitting the attribution of specific daily or weekly excursions to specific process events rather than just the static decomposition reported in this paper. The third is the development of a predictive model that forecasts the expected bin distribution at the end of a production day on the basis of inline parameter measurements earlier in the same day, enabling proactive rather than reactive process intervention. Each of these workstreams is scheduled for progressive delivery during the third and fourth quarters of 2025.

IX - CONCLUSIONS

This paper has presented a production-validated methodology for inline current-voltage curve analysis and binning strategy optimization in PERC solar cell manufacturing, developed at ES Foundry and executed over the April through June 2025 production window. The methodology integrates three analytical disciplines: the decomposition of each measured current-voltage curve into its seven primary electrical parameters, the statistical correlation of these parameters against a suite of upstream process variables, and the quantitative loss decomposition that translates correlation coefficients into fractional contributions to the efficiency loss budget. The combination of these disciplines enables the identification of a small set of high-leverage process variables whose disciplined control produces a measurable shift in the binned efficiency distribution of the production output.
The specific outcomes at ES Foundry over the twelve-week study window are a rise in top-bin yield from six point six percent to thirteen point seven percent of production, a zero point two three percent absolute increase in mean cell efficiency, a narrowing of the efficiency distribution standard deviation from zero point four one to zero point three three percent absolute, and an estimated annualized commercial value of approximately ten point eight million dollars at one gigawatt production scale. The three principal process-variable interventions that drove these outcomes - diffusion recipe revision, laser contact opening width tightening, and firing profile revision - were each identified through the correlation analysis and sequenced for deployment on the basis of their quantitative leverage and the availability of the underlying engineering resource.
The broader generalizable finding is that the flash-test measurement, properly analyzed, is the richest single source of process feedback available in a PERC manufacturing line. Extracting that richness requires the analytical discipline documented in this paper, supported by the manufacturing execution system infrastructure that maintains wafer-level data genealogy from incoming wafer inspection through final binning. Facilities that invest in both the infrastructure and the discipline have available to them a lever on commercial performance whose magnitude is substantial, whose responsiveness is rapid, and whose continued improvement has no near-term ceiling.

X - REFERENCES

[1] Green, M. A. (2009). The path to 25% silicon solar cell efficiency: History of silicon cell evolution. Progress in Photovoltaics, 17(3), 183–189.
[2] Blakers, A. W., Wang, A., Milne, A. M., Zhao, J., & Green, M. A. (1989). 22.8% efficient silicon solar cell. Applied Physics Letters, 55(13), 1363–1365.
[3] Green, M. A., Dunlop, E. D., Hohl-Ebinger, J., Yoshita, M., Kopidakis, N., & Hao, X. (2024). Solar cell efficiency tables (Version 63). Progress in Photovoltaics, 32(1), 3–13.
[4] Nelson, J. (2003). The Physics of Solar Cells. Imperial College Press.
[5] Würfel, P., & Würfel, U. (2016). Physics of Solar Cells: From Basic Principles to Advanced Concepts (3rd ed.). Wiley-VCH.
[6] Schroder, D. K. (2006). Semiconductor Material and Device Characterization (3rd ed.). Wiley-IEEE Press.
[7] Sinton, R. A., & Cuevas, A. (1996). Contactless determination of current–voltage characteristics and minority-carrier lifetimes in semiconductors from quasi-steady-state photoconductance data. Applied Physics Letters, 69(17), 2510–2512.
[8] Montgomery, D. C. (2020). Introduction to Statistical Quality Control (8th ed.). Wiley.

iJETRM
International Journal of Engineering Technology Research & Management (IJETRM)
Journal Article
https://ijetrm.com/issue/

[9] Kane, V. E. (1986). Process capability indices. Journal of Quality Technology, 18(1), 41–52.
[10] Preu, R., Lohmüller, E., Lohmüller, S., et al. (2020). Passivated emitter and rear cell - Devices, technology, and modeling. Applied Physics Reviews, 7(4), 041315.
[11] Dullweber, T., & Schmidt, J. (2016). Industrial silicon solar cells applying the passivated emitter and rear cell (PERC) concept - A review. IEEE Journal of Photovoltaics, 6(5), 1366–1381.
[12] Zhao, J., Wang, A., & Green, M. A. (1999). 24.5% efficiency silicon PERT cells on MCZ substrates. Progress in Photovoltaics, 7(6), 471–474.
[13] Aberle, A. G., Altermatt, P. P., Heiser, G., Robinson, S. J., Wang, A., Zhao, J., Krumbein, U., & Green, M. A. (1995). Limiting loss mechanisms in 23% efficient silicon solar cells. Journal of Applied Physics, 77(7), 3491–3504.
[14] Hoex, B., Schmidt, J., Pohl, P., van de Sanden, M. C. M., & Kessels, W. M. M. (2008). Silicon surface passivation by atomic layer deposited Al2O3. Journal of Applied Physics, 104(4), 044903.
[15] Hannebauer, H., Dullweber, T., Baumann, U., Falcon, T., & Brendel, R. (2014). Fine-line printing options for high efficiencies and low Ag paste consumption. Energy Procedia, 38, 725–731.
[16] IEC 60904-3:2019. Photovoltaic devices - Part 3: Measurement principles for terrestrial photovoltaic solar devices with reference spectral irradiance data. International Electrotechnical Commission.
[17] IEC 60904-1:2020. Photovoltaic devices - Part 1: Measurement of photovoltaic current-voltage characteristics. International Electrotechnical Commission.
[18] IEC 60891:2021. Photovoltaic devices - Procedures for temperature and irradiance corrections to measured I-V characteristics. International Electrotechnical Commission.
[19] Spataru, S., Hacke, P., & Sera, D. (2018). Quantifying solar cell defects and the impact on energy yield using electroluminescence. Solar Energy, 174, 607–617.
[20] Sarver, T., Al-Qaraghuli, A., & Kazmerski, L. L. (2013). A comprehensive review of the impact of dust on the use of solar energy: History, investigations, results, literature, and mitigation approaches. Renewable and Sustainable Energy Reviews, 22, 698–733.
[21] US Department of Energy (2023). Solar Energy Technologies Office: Annual Technology Baseline. National Renewable Energy Laboratory.
[22] Inflation Reduction Act of 2022, Public Law 117-169. Section 45X Advanced Manufacturing Production Credit.
[23] Jordan, D. C., Kurtz, S. R., VanSant, K., & Newmiller, J. (2016). Compendium of photovoltaic degradation rates. Progress in Photovoltaics, 24(7), 978–989.
[24] Haschke, J., Dupré, O., Boccard, M., & Ballif, C. (2018). Silicon heterojunction solar cells: Recent technological development and practical aspects. Solar Energy Materials and Solar Cells, 187, 140–153.
[25] Mack, C. A. (2011). Reducing the manufacturing process variability. IEEE Transactions on Semiconductor Manufacturing, 24(2), 214–220.
[26] Pearson, K. (1896). Mathematical contributions to the theory of evolution - Regression, heredity, and panmixia. Philosophical Transactions of the Royal Society of London A, 187, 253–318.